

Article

Catalytic Ozonation for Effective Degradation of Coal Chemical Biochemical Tail Water by Mn/Ce@RM Catalyst

Yicheng Wang ¹, Yingkun Wang ¹, Xi Lu ², Wenquan Sun ^{1,*}, Yanhua Xu ², Jun Zhou ¹  and Yongjun Sun ^{1,*} 

¹ College of Urban Construction, Nanjing Tech University, Nanjing 211816, China;

chenqu96300@163.com (Y.W.); 15951007013@163.com (Y.W.); zhoujun0913@126.com (J.Z.)

² School of Environmental Sciences and Engineering, Nanjing Tech University, Nanjing 211816, China;

strong_119@126.com (X.L.); xuyh@njtech.edu.cn (Y.X.)

* Correspondence: coneflower@163.com (W.S.); sunyongjun@njtech.edu.cn (Y.S.)

Abstract: An Mn/Ce@red mud (RM) catalyst was prepared from RM via a doping–calcination method. Scanning electron microscopy, X-ray diffraction, and X-ray photoelectron spectroscopy were used to characterize the surface morphology, crystal morphology, and elemental composition of the Mn/Ce@RM catalyst, respectively. In addition, preparation and catalytic ozonation conditions were optimized, and the mechanism of catalytic ozonation was discussed. Lastly, a fuzzy analytic hierarchy process (FAHP) was adopted to evaluate the degradation of coal chemical biochemical tail water. The best preparation conditions for the Mn/Ce@RM catalyst were found to be as follows: (1) active component loading of 3%, (2) Mn/Ce doping ratio of 2:1, (3) calcination temperature of 550 °C, (4) calcination time of 240 min, and (5) fly ash floating bead doping of 10%. The chemical oxygen demand (COD) removal rate was 76.58% under this preparation condition. The characterization results suggested that the pore structure of the optimized Mn/Ce@RM catalyst was significantly improved. Mn and Ce were successfully loaded on the catalyst in the form of MnO₂ and CeO₂. The best operating conditions in the study were as follows: (1) reaction time of 80 min, (2) initial pH of 9, (3) ozone dosage of 2.0 g/h, (4) catalyst dosage of 62.5 g/L, and (5) COD removal rate of 84.96%. Mechanism analysis results showed that hydroxyl radicals (\bullet OH) played a leading role in degrading organics in the biochemical tail water, and adsorption of RM and direct oxidation of ozone played a secondary role. FAHP was established on the basis of environmental impact, economic benefit, and energy consumption. Comprehensive evaluation by FAHP demonstrated that D₃ (with an ozone dosage of 2.0 g/H, a catalyst dosage of 62.5 g/L, initial pH of 9, reaction time of 80 min, and a COD removal rate of 84.96%) was the best operating condition.



Citation: Wang, Y.; Wang, Y.; Lu, X.; Sun, W.; Xu, Y.; Zhou, J.; Sun, Y. Catalytic Ozonation for Effective Degradation of Coal Chemical Biochemical Tail Water by Mn/Ce@RM Catalyst. *Water* **2022**, *14*, 206. <https://doi.org/10.3390/w14020206>

Academic Editor: Mehrab Mehrvar

Received: 1 December 2021

Accepted: 31 December 2021

Published: 11 January 2022

Publisher's Note: MDPI stays neutral with regard to jurisdictional claims in published maps and institutional affiliations.



Copyright: © 2022 by the authors. Licensee MDPI, Basel, Switzerland. This article is an open access article distributed under the terms and conditions of the Creative Commons Attribution (CC BY) license (<https://creativecommons.org/licenses/by/4.0/>).

1. Introduction

Red mud (RM) is the alkaline solid waste discharged during the production of alumina via the Bayer process [1]. RM has a relatively fine particle size (average particle size $\leq 10 \mu\text{m}$), mainly composed of iron, aluminum, sodium, silicon, and titanium oxides [2]. Owing to heavy metals and high alkalinity, the storage and utilization of RM have always been a major environmental challenge. In the past few years, the main way to deal with RM has been on-site stacking [3]. However, this method not only takes up land resources but also causes the harmful components of RM to penetrate the soil and groundwater, causing environmental problems, such as land alkalization and groundwater pollution [4,5]. The current global RM stock is estimated to exceed 4 billion tons, and it is increasing at a rate of 120 million tons per year [6]. Therefore, better strategies are urgently needed to manage RM.

RM contains substantial chemical substances, such as Fe₂O₃, Al₂O₃, TiO₂, and SiO₂, which can be used as adsorbents, coagulants, and catalysts in sewage treatment [7]. Considering its large specific surface area and pore frame structure, RM is also used as a

support for some catalysts, such as Mn, Cu, and Ce oxides [8,9]. Given the limited ability of the original RM to degrade pollutants [10], most research focuses on improving RM to obtain better catalytic activity. A series of treatment methods, including acidification, neutralization, and heat treatment, have been shown to improve the physical and chemical properties of RM [11]. Acidification and neutralization can dissolve calcium salts to create new cavities and increase surface area, thereby increasing the efficiency of RM to degrade pollutants [11,12]. Studies have shown that acidification and roasting of RM at 400 °C can significantly increase its BET surface area and catalytic activity [13]. Manganese-loaded acidified RM can rapidly degrade toluene under ozone conditions [14]. The Ce@RM catalyst prepared using the surface precipitation method can improve the efficiency of degrading bezafibrate [15]. The wastewater produced by the coal chemical industry contains a large amount of ammonia, polycyclic aromatic hydrocarbons, volatile phenols, and benzene series, which are highly toxic and difficult to degrade [16,17]. The efficiency of direct oxidation of coal chemical wastewater by ozone is limited, and the treatment cost is high [18,19]. Thus, the use of an RM catalyst helps improve reaction efficiency and economic benefits. Nevertheless, the preparation scheme for the best RM catalyst for the degradation of coal chemical wastewater remains unclear. At the same time, unsuitable catalytic ozonation reaction conditions may lead to a decrease in the efficiency of the reaction system to degrade pollutants [20].

RM contains a large amount of Fe_2O_3 and Al_2O_3 as common photocatalyst carriers and active components, which are widely used in catalytic oxidation technology to degrade organic pollutants in wastewater. As an advanced technology, catalytic ozonation technology has the advantages of wide application range, fast reaction rate, strong oxidation capacity, and no pollution. It has shown broad application potential in the treatment of water pollutants. On this basis, from the analysis of structure, composition, and stability, RM is suitable as a catalyst or catalyst carrier for high value-added utilization. Designing an efficient and stable ozone catalyst from RM not only enables the recycling of resources but also has significance in protecting the environment. The purpose of this study is to prepare a Mn/Ce@RM catalyst with high economic benefits and good degradation performance. This catalyst can degrade the coal chemical biochemical tail water through a heterogeneous catalytic ozonation system, effectively enhancing the efficiency of the removal of organic pollutants from wastewater during separate ozonation and overcoming the problem of low ozone utilization. At the same time, this work deeply studies the degradation characteristics of organic pollutants in wastewater, operating conditions, catalyst activity and stability, and degradation mechanism to realize a comprehensive evaluation of the RM catalytic ozonation reaction system.

In this study, the Mn/Ce@RM catalyst was prepared from RM via a doping–calcination method. The catalyst was applied to the research of advanced treatment of coal chemical biochemical tail water. Scanning electron microscopy (SEM), X-ray diffraction (XRD), and X-ray fluorescence (XRF) spectroscopy were used to study the structure and apparent properties of the Mn/Ce@RM catalyst. The biochemical tail water was degraded through catalytic ozonation by using the Mn/Ce@RM catalyst. The best operating conditions were determined by optimizing the catalytic ozonation time, ozone dosage, Mn/Ce@RM dosage, and initial pH of wastewater. The stability of the Mn/Ce@RM catalyst was studied. Then, free radical inhibitor (tert-butanol, TBA) test, tail water's ultraviolet full-wavelength scanning (UV-vis), and three-dimensional fluorescence spectroscopy (excitation emission matrix) characterization were performed to explore the heterogeneous catalytic ozonation reaction mechanism. On the basis of environmental impact, economic benefits and energy consumption, with chemical oxygen demand (COD) removal rate, ozone dosage, catalyst dosage, initial pH, and reaction time as evaluation indicators, fuzzy hierarchical analysis of the Mn/Ce@RM catalyst was performed. Comprehensive evaluation of each operating condition was also conducted.

2. Materials and Methods

2.1. Materials

Manganese nitrate, cerium nitrate hexahydrate, sodium bicarbonate, TBA, silver sulfate (Ag_2SO_4), indigo ($\text{C}_{16}\text{H}_{10}\text{O}_2\text{N}_2$), potassium dichromate ($\text{K}_2\text{Cr}_2\text{O}_7$), and soluble starch ($\text{C}_{12}\text{H}_{22}\text{O}_{11}$) are all analytically pure. They were purchased from Nanjing Chemical Reagent Co., Ltd (Nanjing, China). Potassium iodide (KI), sodium thiosulfate ($\text{Na}_2\text{S}_2\text{O}_3$), and ethanol ($\text{C}_2\text{H}_6\text{O}$), which are all analytically pure, were purchased from Sinopharm Chemical Reagent Co., Ltd (Ningbo, China). Fly ash floating beads (100 mesh) and attapulgite (400 mesh) were purchased from Henan Borun Casting Material Co., Ltd (Pingdingshan, China). RM was collected from an alumina production plant in Chongqing. The XRF characterization results of the RM raw materials are shown in Table S1. The wastewater used in the experiment was coal chemical biochemical tail water, taken from a sewage treatment plant in an industrial park. From the apparent appearance, the tail water has high chromaticity and turbidity, and the water contains black solid suspended solids. The raw water quality test results and measurement methods are shown in Table 1.

Table 1. Water quality analysis of experimental water.

Index	Unit	Content	Method
COD	mg/L	287.23	Potassium dichromate method
Ammonia nitrogen	mg/L	0.82	Nessler's reagent colorimetric method
pH	/	7.3	Glass electrode method
Turbidity	NTU	12.75	Photoelectric turbidimeter
Total nitrogen	mg/L	1.37	Alkaline potassium persulfate digestion UV spectrophotometric method
TOC	mg/L	95.16	TOC analyzer
Colority	PCU	122.2	High-precision colorimeter
Total Phosphorus	mg/L	0.98	Ammonium molybdate spectrophotometric method

2.2. Preparation of Supported Catalyst

The RM was baked in an oven at 105 °C for 24 h, the dried RM was ground through a sieve, and the particle size was controlled to 0.12–0.15 mm. Quantitative amounts of $\text{Mn}(\text{NO}_3)_2$, $\text{Ce}(\text{NO}_3)_3 \cdot 6\text{H}_2\text{O}$, $\text{Bi}(\text{NO}_3)_3 \cdot 5\text{H}_2\text{O}$, $\text{Cu}(\text{NO}_3)_2 \cdot 6\text{H}_2\text{O}$, and $\text{Ni}(\text{NO}_3)_2 \cdot 6\text{H}_2\text{O}$ were weighed, and 100 mL of nitrate solution was prepared as active component. The component precursors were placed in a beaker for later use. Next, 100 g of pretreated RM, 15 g of attapulgite, and a certain amount of pore former were weighed, placed in a mortar, and stirred evenly. The quantitative active component precursor and deionized water were added to the mortar, stirred to make the medium uniformly mixed, and placed in an oven at 60 °C for 3 h. The particle size of the RM catalyst pellets was controlled to 4–6 mm, and they were placed in an oven at 60 °C for 24 h. The dried RM catalyst was placed in a crucible and then in a muffle furnace, roasted at a certain temperature for a certain period of time and taken out after the roasting to obtain the Mn/Ce@RM catalyst [18].

2.3. Catalyst Characterization Method

A scanning electron microscope (ZEISS Merlin, Zeiss, Oberkochen, Germany) was used to characterize the apparent morphology of the catalyst. An X-ray diffractometer (D8 Advance, Bruker, Karlsruhe, Germany) was used to characterize the crystal morphology of the supported metal inside the catalyst. An XRF spectroscope (Axios Pw4400, PANalytical B.V., Almelo, The Netherlands) was used to characterize the content of metal elements and oxides inside the catalyst. An analyzer for specific surface area, pore distribution, and adsorption performance (Micromeritics, ASAP2020, Atlanta, GA, USA) was used to characterize the pore volume, pore size, and adsorption performance of the catalyst. An X-ray photoelectron spectroscopy (XPS) analyzer (Escalab250, Thermo Scientific, Waltham, MA, USA) was used to characterize the surface element composition of

the catalyst. An energy-dispersive X-ray spectroscope (Kratos AXIS Ultra DLD, Shimadzu Corporation, Tokyo, Japan) was used to characterize the distribution of various elements in the catalyst [18].

2.4. Experimental Device and Process

To investigate the adsorption of RM on organics in the biochemical tail water, 20 g of a blank RM catalyst was added to the reactor, 400 mL of biochemical tail water was added, and the ozone generator and aeration equipment were turned off. The reaction time was 180 min, and water samples were collected every 20 min. The COD removal rate was used as an evaluation indicator to study the adsorption performance of the blank RM catalyst. The catalytic ozonation reactor (ozone generator, CF-G-3-10G, Qingdao Guolin Environmental Protection Technology Co., Ltd., Qingdao, China) and its operation process are shown in Figure S1. The reactor is a cylindrical container made of plexiglass (with a volume of 500 mL). Before the start of the experiment, 400 mL of biochemical tail water was first removed to be processed into the reactor, and a quantitative Mn/Ce@RM catalyst was added. The high-purity oxygen cylinder was opened, and the outlet pressure was adjusted to 0.12 MPa through the pressure-reducing valve. The condensing water device and the ozone generator were turned on, the principle of high-voltage discharge was used to convert oxygen into ozone and pass it into the reactor through the air diffuser, and the degradation experiment was started. Water samples were collected every 10 min, and the exhaust gas produced was discharged outdoors after two-stage 20% KI solution absorption treatment. The ozone concentration in the gas phase was determined using the iodometric method [21]. The indigo decolorization method was used to determine the ozone concentration in the liquid phase [18]. Three-dimensional fluorescence spectroscopy (excitation emission matrix, EEM) of the biochemical tail water was performed with a fluorescence spectrophotometer (F7000, Hitachi Company, Tokyo, Japan). The test conditions were as follows: emission wavelength of 270–600 nm, excitation wavelength of 250–450 nm, slit width of 5 nm, and emission laser scanning step length of 2 nm. The water samples were tested and analyzed using UV-Vis technology (ultraviolet spectrophotometer, UV-5500, Shanghai Yuanxi Instrument Co., Ltd., Shanghai, China).

2.5. Fuzzy Hierarchical Structure Model

To determine the optimal catalyst and operating conditions for the experiment, the analytic hierarchy process (AHP) was used to construct a hierarchical model. The target layer was determined as “Mn/Ce@RM catalyst comprehensive evaluation” and named M. Environmental impact (I), economic benefit (B), and energy consumption (C) were selected as the evaluation layer. Five indicators existed in the indicator layer. The COD removal rate I_1 was selected as the environmental impact indicator; the ozone dosage B_1 , catalyst dosage B_2 , and initial pH B_3 were used as economic efficiency indicators; and the reaction time C_1 was used as the energy consumption indicator [22]. The structure diagram of the comprehensive evaluation index system of the Mn/Ce@RM catalyst is shown in Figure S2. This article used the expert scoring method to determine the index weight and compared the indexes pair by pair on a scale of 1–9. The specific comparison method is shown in Table S2. In accordance with the 1–9 scale method, the importance of each index of the evaluation layer was compared. If a certain evaluation layer had n indexes $A_1, A_2, A_3, \dots, A_n$, then b_{ij} was used to represent the ratio of the influence of indexes A_i and A_j on the evaluation layer. The structure of the pairwise judgment comparison matrix is shown in Table S3. Text S1 presents the calculation of index weight and consistency check, the calculation of index membership, and the structure of factor evaluation set R.

3. Results and Discussions

3.1. Mn/Ce@RM Catalyst Preparation Optimization

As shown in Figure 1a, under ozone-free conditions, the blank RM catalyst has a fast adsorption rate within 0–60 min and reaches the adsorption saturation state at 80 min,

and the COD removal rate is 7.89%. In the ozonation reaction system alone, the COD removal rate remains stable after 80 min, which is 31.14%. Compared with ozonation alone, the COD removal rate increases after adding the blank RM catalyst and finally reaches 36.58%. As shown in Figure 1b, compared with the RM catalyst with a single active component, the incorporation of Mn and Ce considerably improves the degradation performance of the catalyst. In addition, the Mn/Ce@RM catalysts prepared with different Mn:Ce doping ratios show distinct catalytic activities. When Mn:Ce = 1:4, the COD removal rate is low. With the increase in the doping ratio of Mn, the COD removal rate continues to rise. When Mn:Ce = 2:1, the COD removal rate reaches the maximum value of 59.07% in the experiment. However, when the doping ratio of Mn continues to increase, the degradation of the Mn/Ce@RM catalyst on the biochemical tail water gradually worsens. When Mn:Ce = 4:1, the COD removal rate drops to 55.01%. Figure 1c shows that when the calcination temperature is 350–550 °C, with the increase in calcination temperature, the performance of the Mn/Ce@RM catalyst is significantly improved, and the COD removal rate increased from 47.38% to 64.38%. Nonetheless, when the temperature is increased to 600 °C, the performance of the Mn/Ce@RM catalyst decreases slightly, and the COD removal rate drops to 57.24%. As shown in Figure 1d, when the calcination time is 150–240 min, the performance of the Mn/Ce@RM catalyst shows a significant improvement with time, and the COD removal rate increases from 51.38% to 66.93%. The degradation performance of the catalyst shows a slight decrease when calcination time over 240 min. When the calcination time is 300 min, the COD removal rate drops to 63.31%.

3.2. Characterization of the Mn/Ce@RM Catalyst

As shown in Figure 2a, the morphology of the blank RM is mainly granular and massive, the surface is rough and uneven. A few uneven pores exist in the blank RM and the pore size is not uniform. According to Figure 2b, after fly ash float beads are added, the pore structure of the Mn/Ce@RM catalyst is improved significantly, the number of pores increases, the particle distribution is uniform, and a large amount of metal oxides are attached. At the same time, the components are tightly combined without agglomeration. Figure 2c shows the SEM characterization of the Mn/Ce@RM catalyst reused 25 times. The pore connectivity of the catalyst is significantly reduced after repeated use. This may be due to the clogging of the pores by pollutants or the collapse of the pores caused by aeration during the degradation [23]. As shown in Table 2 and Figure S3, the specific surface area of the optimal Mn/Ce@RM catalyst is 12.1829 m²/g, which is 1.97 times the specific surface area of the blank RM (6.1959 m²/g). The expansion of the specific surface area can improve the adsorption performance of the catalyst, prolong the residence time of ozone in the wastewater, and thus improve the catalytic efficiency [24]. The specific surface area, specific pore volume, and average pore diameter of the Mn/Ce@RM catalyst are reduced after reusing 25 times, which are 11.5218 m²/g, 0.0684 cm³/g, and 3.5716 nm, respectively.

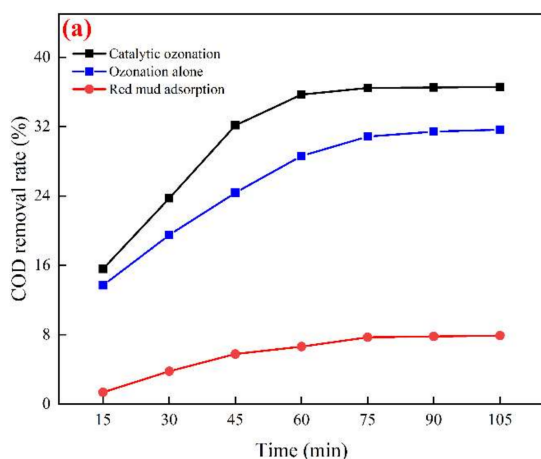


Figure 1. Cont.

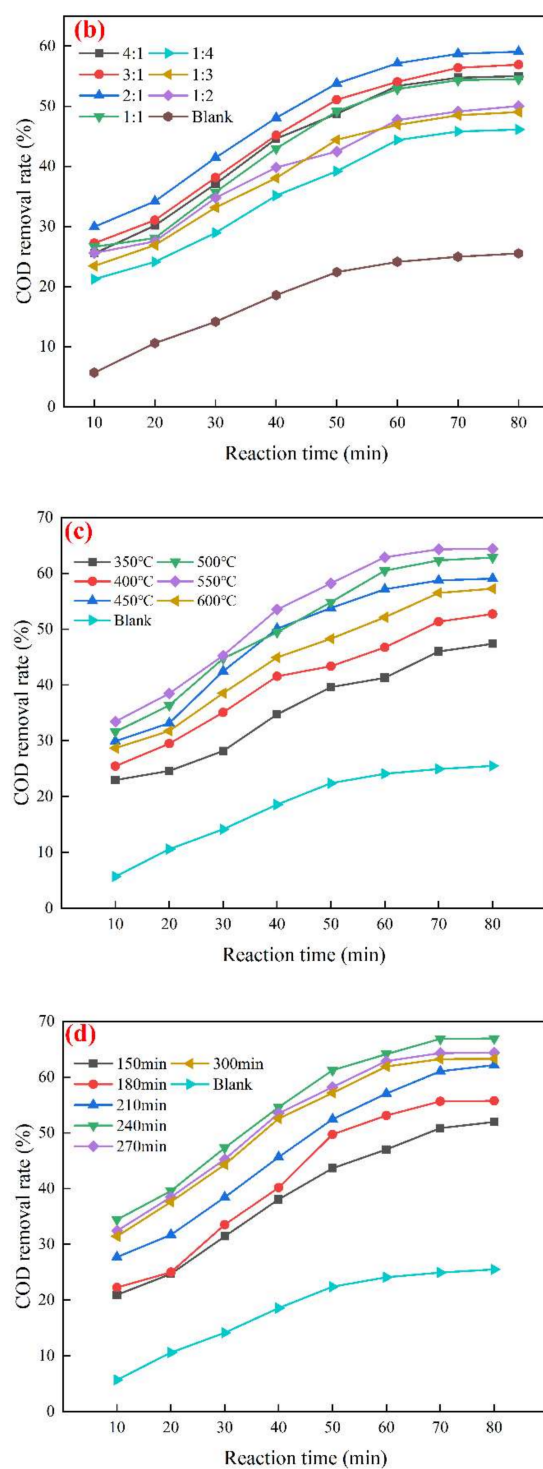


Figure 1. Effect of different preparation conditions on COD removal rate: (a) Effect of different reaction systems on COD removal rate; (b) Effect of Mn:Ce doping ratio on COD removal rate, (c) Effect of roasting temperature on COD removal rate; (d) Effect of roasting time on COD removal rate.

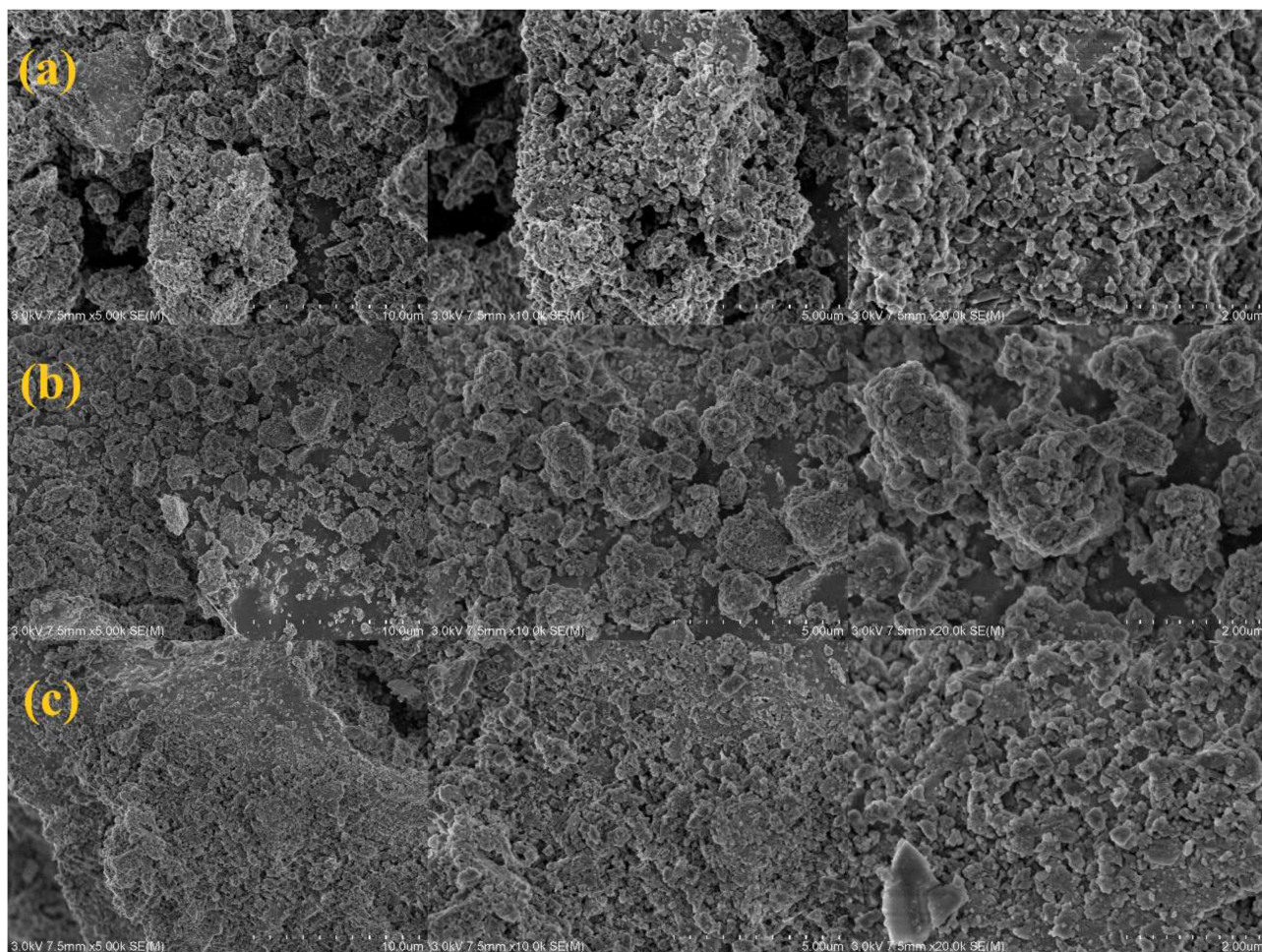


Figure 2. SEM characterization results: (a) Red mud blank sample; (b) Mn/Ce@RM catalyst (Fly ash floating beads); (c) Mn/Ce@RM catalyst reused 25 times.

Table 2. Pore structure characteristics of different materials.

Materials	Red Mud Blank Sample	Mn/Ce@RM Catalyst	Mn/Ce@RM Catalyst Reused 25 Times
Specific surface area (m^2/g)	6.1959	12.1829	11.5218
Specific pore volume (cm^3/g)	0.0401	0.0722	0.0684
Average pore diameter (nm)	5.1724	3.6185	3.5716

Figure 3a demonstrates that the main constituent elements of RM include Al (16.61 wt%), Si (10.12 wt%), Fe (37.41 wt%), Mn (0.07 wt%), and Ce is not detected. Figure 3b shows that the content of Al, Si, and Fe in the catalyst prepared using the doping–calcination method is reduced to 15.21, 7.59, and 35.46 wt%, respectively. By contrast, the content of Mn and Ce is significantly increased to 1.52 and 0.73 wt%, respectively. Figure 3c presents that after repeated use, the active components in catalyst fall off slightly [25]. The possible reasons for the loss of active components include the collision of the Mn/Ce@RM catalyst and the continuous erosion of the catalyst surface by aeration.

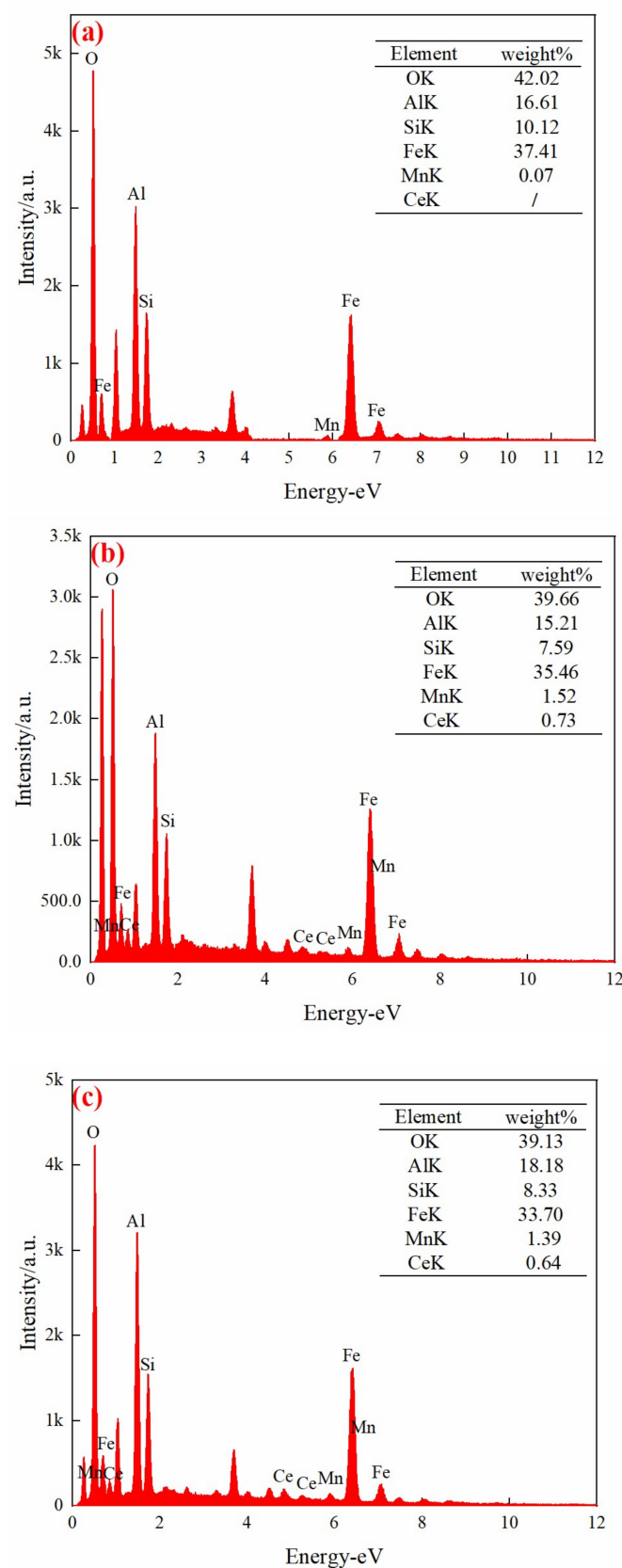


Figure 3. EDS characterization results: (a) Red mud blank sample; (b) Optimal Mn/Ce@RM catalyst sample; (c) Mn/Ce@RM catalyst reused 25 times.

Table 3 shows that Fe_2O_3 , SiO_2 , and Al_2O_3 are the main components in the blank sample of RM, and their contents are 39.32, 12.23, and 25.37 wt%, respectively. The remaining components include CaO , Na_2O , TiO_2 , and a trace amount of MnO_2 . Compared with the blank sample of RM, the content of MnO_2 and CeO_2 in the optimal sample of Mn/Ce@RM catalyst increased to 1.69 and 0.75 wt%, respectively. After the Mn/Ce@RM catalyst is used 25 times, the content of MnO_2 and CeO_2 decreased by 0.11 and 0.07 wt%, respectively. In addition, the active components, such as Fe and Ti, contained in the RM will form $\text{Fe}_2\text{O}_3\text{-MnO}_2$, $\text{TiO}_2\text{-MnO}_2$, $\text{Fe}_2\text{O}_3\text{-CeO}_2$, $\text{TiO}_2\text{-CeO}_2$, and other multicomponent synergistic catalytic degradation systems with the oxides of Mn and Ce [18]. Such formation will further improve the performance of the Mn/Ce@RM catalyst to degrade biochemical tail water.

Table 3. XRF characterization results (wt%).

	CaO	Al_2O_3	SiO_2	Na_2O	TiO_2	Fe_2O_3	MnO_2	CeO_2
Red mud blank sample	5.05	25.37	12.23	7.65	4.54	39.32	0.12	/
Optimal Mn/Ce@RM catalyst sample	4.41	25.19	19.04	6.73	4.18	35.02	1.69	0.75
Mn/Ce@RM catalyst reused 25 times	4.49	25.15	18.44	6.33	4.19	31.06	1.57	0.68

As shown in Figure 4a, the blank sample of RM has evident characteristic peaks at $2\theta = 27.4^\circ$, 33.1° , 37.1° , which are Fe_2O_3 , TiO_2 , and Al_2O_3 , respectively. Comparison of the diffraction peaks of each catalyst and the blank RM shows that the diffraction peaks of other catalyst samples at $2\theta = 28.1^\circ$, 38.1° , 43.2° , 56.7° are consistent with MnO_2 , and the diffraction peaks at $2\theta = 29.2^\circ$ and 45.5° are consistent with CeO_2 . This finding indicates that the Mn and Ce in the Mn/Ce@RM catalyst mainly exist in the crystalline phase of MnO_2 and CeO_2 . Compared with the Mn/Ce@RM catalyst prepared at 500 and 550 °C, the diffraction peaks of the catalyst obtained at 400 and 450 °C have lower intensity at $2\theta = 28.1^\circ$, 29.2° , 38.1° , 45.5° . This result indicates that the calcination temperatures of 400 and 450 °C are inconducive to the formation of MnO_2 and CeO_2 crystal phases. With the increase in calcination temperature, the intensity of each characteristic diffraction peak also gradually increases. The crystallinity of Mn and Ce is further improved and reaches the best when the calcination temperature is 550 °C.

As shown in Figures 4b and S4, the characteristic peaks of Al, Si, Ca, Fe, Na, O, and other elements are detected in the blank sample of RM, but Mn and Ce are not detected. Relatively sharp characteristic peaks exist for Mn and Ce, indicating that the active components have been successfully supported on the catalyst in the form of MnO_2 and CeO_2 . The XPS full spectrum of the Mn/Ce@RM catalyst after 25 times of repeated use shows that the characteristic peaks of Mn and Ce do not appear to be significantly weakened, indicating that the loss of active components of the catalyst after repeated use is minimal.

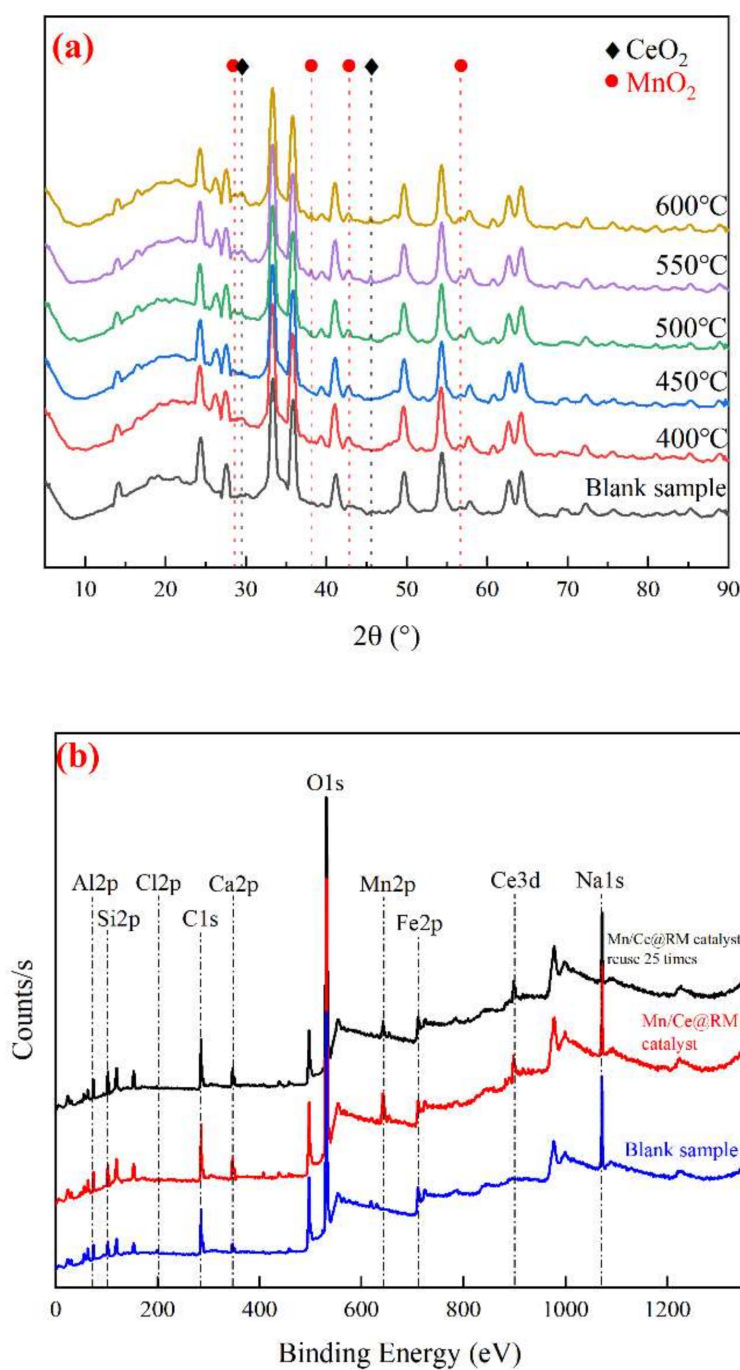


Figure 4. (a) XRD characterization results; (b) XPS characterization results: XPS full spectrum.

3.3. Study on the Best Operating Conditions for Catalytic Ozonation and Catalyst Stability

Figure 5a depicts that the COD removal rate rises rapidly from 0% to 72.33% at 0–80 min. It rises slowly after 80 min, and the COD removal rate at 160 min is 73.53%, which is only 1.20% higher than the removal rate at 80 min. The possible reason is that the concentration of organic matter at the beginning of the reaction is relatively high. Active oxygen-containing groups, such as $\bullet\text{OH}$, produced by catalytic ozonation can rapidly degrade organic matter, such that the removal rate of COD increases significantly. As the reaction time is prolonged, a large amount of organic matter has been degraded in the early stage, and the concentration of organic matter is lower, which may lead to a slow increase in the COD removal rate in subsequent experiments. Therefore, from the experiments, the optimal reaction time is 80 min.

As shown in Figure 5b, when the ozone dosage is increased from 1.2 to 2.0 g/h, the COD removal rate at 80 min rises from 57.38% to 75.68%, an increase of 18.3%. However, when the ozone dosage continues to be increased from 2.0 to 2.8 g/h, the increase is only 2.43%. When the intake air volume is low, the amount of ozone dissolved in the water can be increased by increasing the intake air volume. The Mn and Ce in the Mn/Ce@RM catalyst can fully contact the liquid phase ozone, thereby improving the degradation efficiency of the biochemical tail water [26]. Nevertheless, when the dosage of ozone > 2.0 g/h, the hydraulic residence time of ozone in the water increases correspondingly, the utilization rate of ozone decreases, and the rate of OH generation is slowed down, resulting in a small increase in COD removal rate [27]. In addition, excessive ozone dosage will cause ozone to be directly discharged from the reaction system. Considering the efficiency and economic benefits of the reaction system, 2.0 g/h is selected as the optimal ozone dosage.

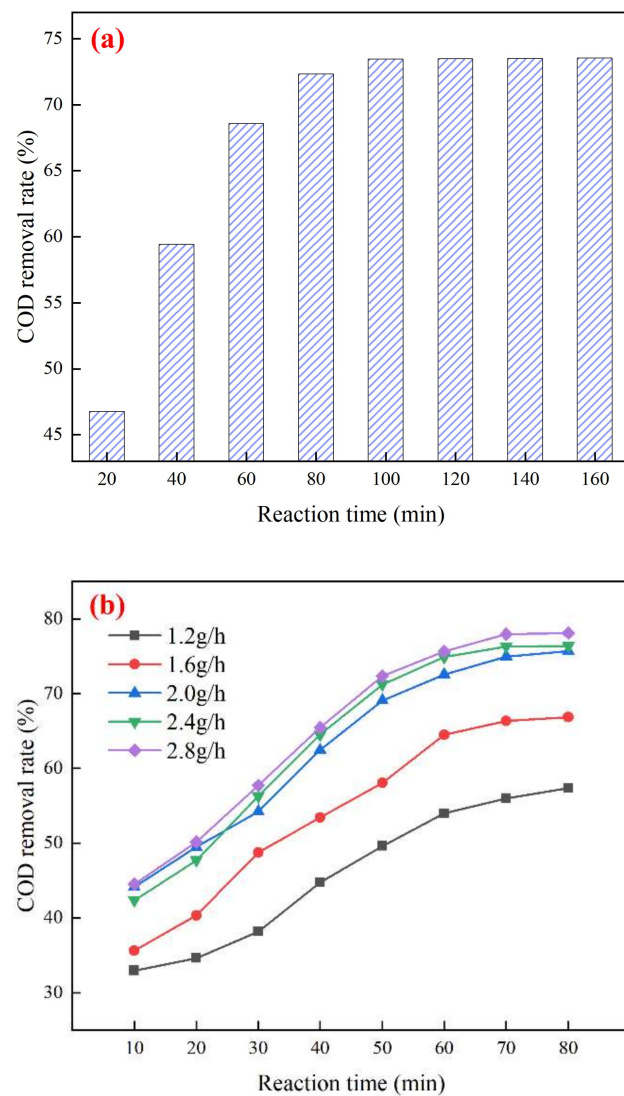


Figure 5. Cont.

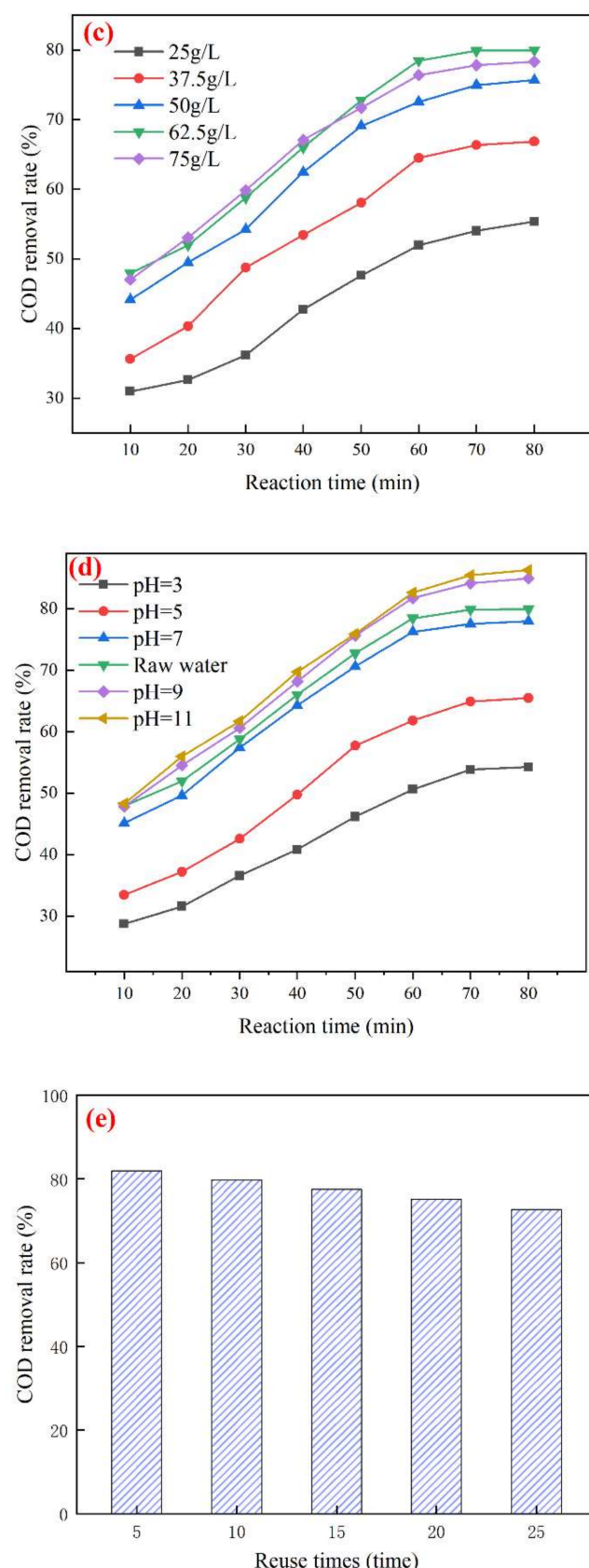


Figure 5. Experimental results of optimum operation in catalytic ozonation and catalyst stability: (a) Effect of reaction time on COD removal rate; (b) Effect of ozone dosage on COD removal rate; (c) Effect of catalyst dosage on COD removal rate; (d) Effect of initial pH on COD removal rate; (e) Effect of catalyst reused times on COD removal rate.

In Figure 5c, when the catalyst dosage is increased from 25 to 62.5 g/L, the COD removal rate at 80 min increases from 55.38% to 79.95%. Nonetheless, when the catalyst dosage is increased to 75 g/L, the COD removal rate drops to 78.32% at 80 min. When the dosage of the Mn/Ce@RM catalyst increases, the contact of ozone, biochemical tail water, and Mn/Ce@RM catalyst in the reactor increase, which improves the mass transfer efficiency of ozone and the generation of $\bullet\text{OH}$ [28,29]. However, when the dosage of the Mn/Ce@RM catalyst exceeds 62.5 g/L, the excess catalyst may overlap, which reduces the active sites that can contact ozone [30]. Consequently, the degradation performance of the system decreases. Moreover, due to the constant dosage of ozone in the system, the excess Mn/Ce@RM catalyst has more active sites than required for ozone decomposition, resulting in a certain number of catalysts failing to exert their effect in the reaction and increasing operating costs [20]. In summary, 62.5 g/L is selected as the optimal dosage of the Mn/Ce@RM catalyst.

Figure 5d illustrates that when the initial pH value increases from 3 to 9, the COD removal rate in 80 min increases from 54.28% to 84.96%, an increase of 30.68%. Nonetheless, when the initial pH continues to increase to 11, the removal rate only increases by 1.38% compared with that when pH = 9. The decomposition of ozone under acidic conditions is strongly inhibited, resulting in low degradation efficiency. The degradation efficiency is higher under alkaline conditions because Fe-OH and other complexes are more easily formed on the catalyst surface, which contributes to the generation of hydroxyl radicals [31,32]. Ozone is also easier to decompose under alkaline conditions, and the generation rate of OH is increased, which promotes the degradation of pollutants [33,34]. In summary, the best initial pH = 9.

As shown in Figure 5e, as the number of uses increases, the degradation of the Mn/Ce@RM catalyst on the biochemical tail water decreases slightly. After 25 times of repeated use, the COD removal rate is 72.72%, which is only 11.21% lower than the COD removal rate at the initial stage of use. The decrease in activity may be due to the collision and friction among the Mn/Ce@RM catalyst particles during long-term use, which reduces and separates the surface active components. It may also be because in the process of degrading the biochemical tail water, certain substances in the environment remain and accumulate in the catalyst for a long time. As a result, the pore connectivity of the Mn/Ce@RM catalyst deteriorates, and its performance decreases.

3.4. Mechanism Analysis of Catalytic Ozonation Degradation

3.4.1. Effect of TBA on the Degradation Performance of Biochemical Tail Water

As shown in Figure 6, after adding different concentrations of TBA to the two systems, the degradation efficiency is significantly reduced, and the COD removal rate in ozonation alone is relatively less affected by the amount of TBA added. Figure 6a shows that when 0–80 mg/L of TBA is added during ozonation alone, the COD removal rate is reduced from 32.75% to 25.74%, a decrease of 7.01%. When the dosage of TBA is 100 mg/L, the COD removal rate is 25.09%, which is only 0.65% compared with that when the dosage is 80 mg/L. From Figure 6b, after 0–80 mg/L of TBA is added to the catalytic ozonation system, the COD removal rate decreases from 83.47% to 58.72%, a decrease of 24.75%. When the dosage of TBA is 100 mg/L, the COD removal rate continues to decrease, which is 56.98%.

In an ozonation alone system, on the basis of direct oxidation of ozone and indirect oxidation of a small amount of OH generated by ozone decomposition, the degradation of organic matter is realized. With the increase in TBA in this system, the COD removal rate decreases. However, when the dosage of TBA is more than 80 mg/L, the decrease in COD removal rate is significantly reduced, indicating that the $\bullet\text{OH}$ in the system has been completely captured by TBA. At this time, the removal of organic matter completely depends on the direct oxidation of ozone [35]. Nevertheless, after TBA is added to the Mn/Ce@RM catalyst/O₃ system, although the COD removal rate is greatly reduced, it is still much higher than that of the ozonation system alone. This result shows that the

existence of the Mn/Ce@RM catalyst is indeed conducive to the generation of OH [36]. In this system, the oxidation of OH plays a leading role, and the direct oxidation of ozone plays a secondary role. When the dosage of TBA > 80 mg/L, the COD removal rate in the Mn/Ce@RM catalyst/O₃ system remains relatively high. This condition indicates that the adsorption of RM can also remove a part of the organic matter, thereby improving the degradation efficiency of biochemical tail water. The research results show that TBA will have an adverse effect on the generation of •OH [37], and the active components loaded in the Mn/Ce@RM catalyst will promote ozone decomposition to produce more •OH, thereby increasing the COD removal rate. This finding indirectly proves that the Mn/Ce@RM catalytic ozonation follows the free radical mechanism [38].

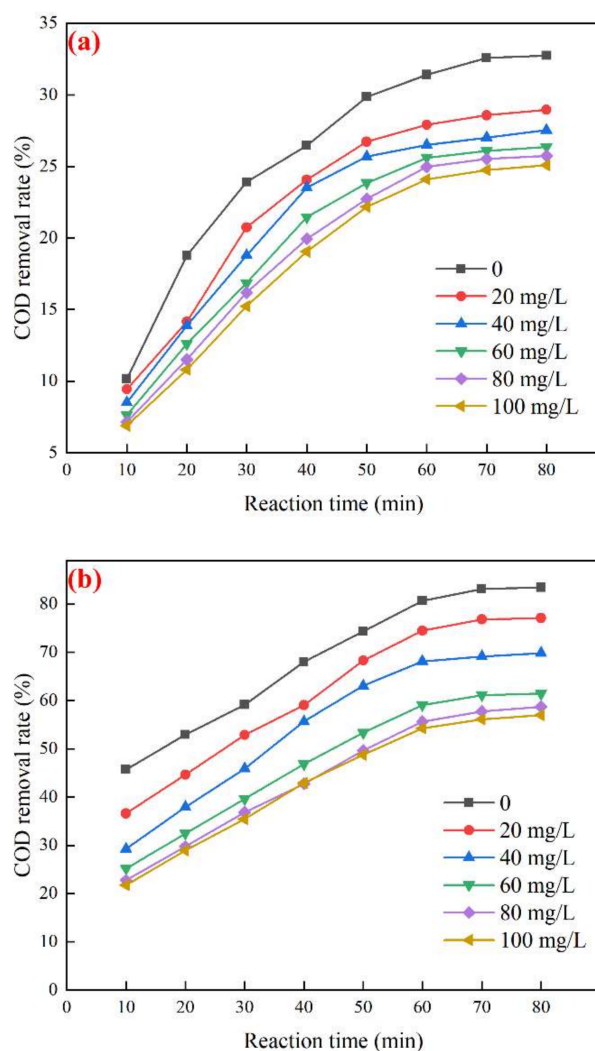


Figure 6. Effect of TBA dosage on COD removal rate: (a) ozonation alone, (b) catalytic ozonation.

3.4.2. UV Absorption Peak of Biochemical Tail Water

Figure 7 illustrates that the biochemical tail water has evident UV absorption peaks at 190–230 nm and 300 nm, of which 190–230 nm is the characteristic waveband of organic acids and aromatic compounds, and 300 nm is the characteristic waveband of polycyclic aromatic hydrocarbons. Accordingly, substantial refractory aromatic compounds exist in raw water. When the reaction is carried out for 10 min, the absorption peak at 190–230 nm is significantly reduced. On the contrary, the absorption peak at 300 nm exceeds that of raw water, which may be due to the destruction of unsaturated bonds during the degradation of aromatic compounds and the cracking of the benzene ring to generate a large amount of intermediate product. With the progress of catalytic ozonation, the intensity of the

absorption peak at 190–230 nm continues to decrease, and the absorption peak at 300 nm basically disappears. Hence, most of the aromatic compounds in the biochemical tail water have been degraded [39]. In addition, after the reaction proceeds for 70 min, the UV absorbance decreases slightly, indicating that most of the aromatic compounds have been degraded [40].

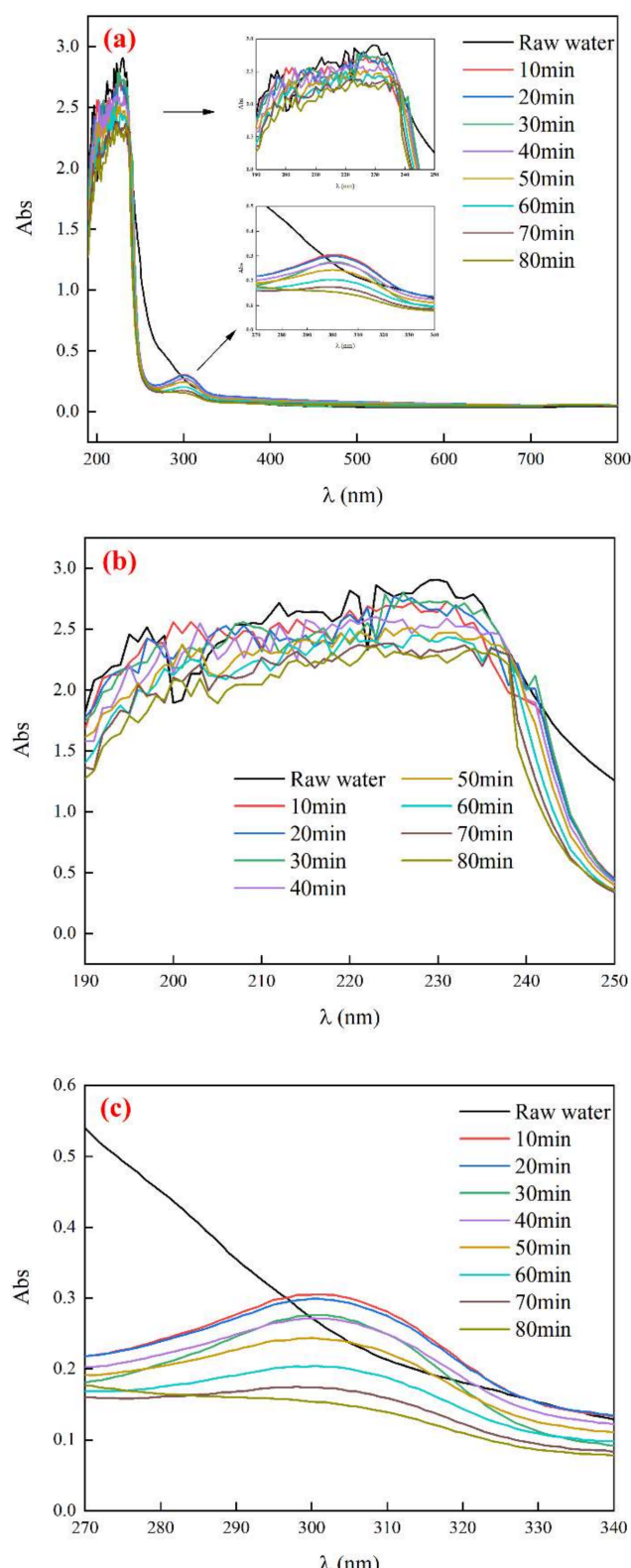


Figure 7. UV-Vis analysis results: (a) 190~800 nm, (b) 190~250 nm, (c) 270~340 nm.

3.4.3. EEM Spectrum Analysis of Biochemical Tail Water

As shown in Figure 8a, a strong fluorescence peak with a larger peak (peak I, Ex/Em = 340–380 nm/370–460 nm) and a weak fluorescence peak with a smaller peak (peak II, Ex/Em = 350–370 nm/290–310 nm) exist. The fluorescent organics in raw water mainly include microbial metabolic by-products (peak II), aromatic substances, and other functional groups containing more carbonyl and carboxyl groups and humus (peak I). As shown in Figure 8b, after 80 min of degradation, the organic composition of the biochemical tail water changes significantly. The fluorescence peak intensity of peaks I and II in the three-dimensional fluorescence spectrum basically disappears, indicating that the Mn/Ce@RM catalytic ozonation and can efficiently degrade fluorescent organics in biochemical tail water. Some weak fluorescence peaks (peak III, Ex/Em = 325 nm/500 nm) remain in the spectrum, which may be due to the formation of intermediate products during the degradation of macromolecular organics in the biochemical tail water. The limited reaction time causes such substances to remain in wastewater.

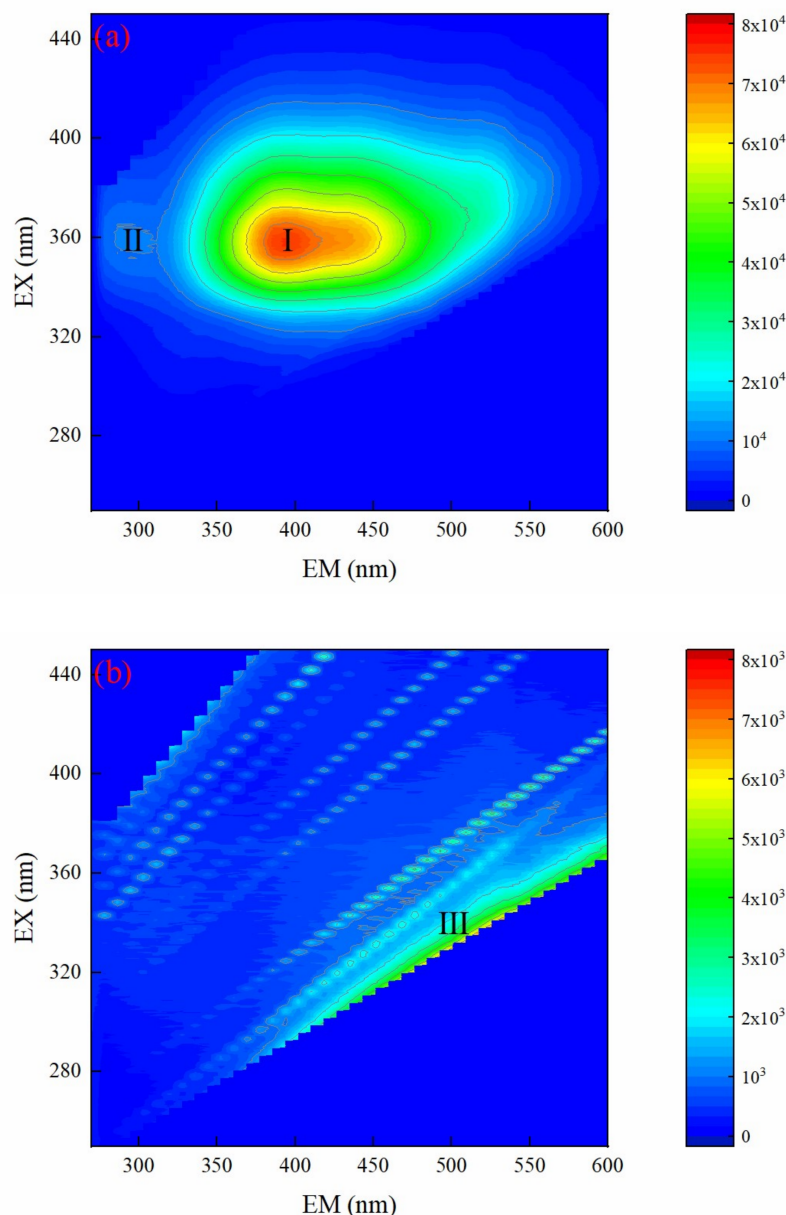


Figure 8. EEM analysis results: (a) raw water (b) degraded for 80 min.

3.5. Fuzzy AHP

From Table 4, the highest score in this evaluation is the D₃ operating condition (the operating conditions are as follows: ozone dosage of 2.0 g/h, catalyst dosage of 62.5 g/L, initial pH of 9, reaction time of 80 min, and COD removal rate of 84.96%). This operating condition has the lowest environmental impact, higher economic benefits, and lowest energy consumption. Next to D₃ is C₁ operating condition (the operating condition are as follows: ozone dosage of 2.0 g/h, catalyst dosage of 37.5 g/L, initial pH of 7.3 (raw water), reaction time of 80 min, and COD removal rate of 67.84%). Although this operating condition has the highest economic benefit, the environmental impact is relatively large. A comprehensive comparison of the environmental impact, economic benefits, and energy consumption of each operating condition shows that D₃ operating condition shows excellent performance, such that it is the best operating model.

Table 4. Comprehensive evaluation score and ranking of each operating condition.

Operating Condition	Environmental Impact I	Economic Benefit B	Fog C	Comprehensive Evaluation Score	Rank
A ₁	0.0513	0.2714	0.2000	0.5226	7
A ₂	0.0578	0.2714	0.0993	0.4285	10
A ₃	0.0581	0.2714	0.0493	0.3788	11
A ₄	0.0582	0.2714	0.0245	0.3541	12
B ₁	0.0272	0.4014	0.2000	0.6286	3
B ₂	0.0735	0.2714	0.2000	0.5449	5
B ₃	0.0793	0.2259	0.2000	0.5052	8
C ₁	0.0316	0.4014	0.2000	0.6330	2
C ₂	0.0840	0.2714	0.2000	0.5554	4
C ₃	0.1165	0.2259	0.2000	0.5424	6
D ₁	0.0245	0.1190	0.2000	0.3435	13
D ₂	0.0845	0.1512	0.2000	0.4357	9
D ₃	0.2000	0.2945	0.2000	0.6945	1

4. Conclusions

In this study, a highly efficient and stable Mn/Ce@RM catalyst was prepared from RM using a doping–calcination method. The COD removal rate was used as an evaluation index to establish a heterogeneous catalytic ozonation system for degradation of coal chemical biochemical tail water. The optimal preparation conditions of the Mn/Ce@RM catalyst were as follows: element doping amount of 3%, Mn and Ce compounding ratio of 2:1, calcination temperature of 550 °C, calcination time of 240 min, and COD removal rate of 66.93%. SEM characterization showed that the pore channels of the Mn/Ce@RM catalyst were significantly increased, the pore structure was greatly improved, and the components were tightly combined without agglomeration. Mn and Ce were successfully supported on the Mn/Ce@RM catalyst, the contents of which were 1.52 and 0.73 wt%, respectively. The supported valence states of Mn and Ce were mainly Mn⁴⁺ and Ce⁴⁺, and the supported forms were MnO₂ and CeO₂. After the Mn/Ce@RM catalyst was reused for 25 times, the biochemical tail water could still maintain a high degradation efficiency, and the COD removal rate was 72.72%. The organic matter in the biochemical tail water was mainly aromatic compounds, by-products of microbial metabolism, and humus-like substances. •OH played a leading role in the degradation of organic matter in the biochemical tail water. Fuzzy hierarchical model analysis showed that the best operating model was D₃ operating condition (with an ozone dosage of 2.0 g/h, a catalyst dosage of 62.5 g/L, initial pH of 9, reaction time of 80 min, and a COD removal rate of 84.96%).

Supplementary Materials: The following supporting information can be downloaded at: <https://www.mdpi.com/article/10.3390/w14020206/s1>; Figure S1: Ozone catalytic reaction flow chart; Figure S2: Comprehensive evaluation index system of Mn/Ce@RM catalyst; Figure S3: BET characterization results: (a) Red mud blank sample, (b) Optimal Mn/Ce@RM catalyst sample, (c) Mn/Ce@RM

catalyst reuse 25 times; Figure S4: XPS characterization results: (a) XPS full spectrum, (b) Mn peak fitting, (c) Ce peak fitting; Table S1: XRF characterization of red mud (wt %); Table S2: Scale method; Table S3: Construction of pairwise comparison matrix; Table S4: The value standard of RI; Table S5: Judgment matrix of evaluation layer to target layer and single ranking result; Table S6: Judgment matrix and single ranking result of index layer's impact on Environment; Table S7: The judgment matrix of economic benefit in index level and the result of single rank; Table S8: Judgment matrix and single ranking result of energy consumption in index layer; Table S9: The total ranking weight of each index layer; Table S10: Comprehensive evaluation index classification of Mn/Ce@RM based ozone catalyst; Table S11: Qualitative index evaluation standard; Table S12: Summary of experimental results; Text S1: The calculation of index weight and consistency check, the calculation of index membership, and the structure of factor evaluation set R.

Author Contributions: Conceptualization, Y.W. (Yicheng Wang), X.L., W.S., Y.X., J.Z. and Y.S.; methodology, X.L., W.S., Y.X., J.Z. and Y.S.; software, W.S. and Y.S.; validation, W.S. and Y.S.; formal analysis, Y.W. (Yingkun Wang) and Y.S.; investigation, Y.W. (Yicheng Wang) and X.L.; resources, W.S. and Y.S.; data curation, Y.W. (Yingkun Wang), X.L., W.S., Y.X., J.Z. and Y.S.; writing—original draft preparation, Y.W. (Yingkun Wang), W.S. and Y.S.; writing—review and editing, W.S. and Y.S.; visualization, W.S. and Y.S.; supervision, W.S. and Y.S.; project administration, W.S. and Y.S.; funding acquisition, W.S. and Y.S. All authors have read and agreed to the published version of the manuscript.

Funding: This research was funded by National Natural Science Foundation of China (no. 51508268), National Natural Science Foundation of China (no. BK20201362), and 2018 Six Talent Peaks Project of Jiangsu Province (JNHB-038).

Data Availability Statement: Data is contained within the article or supplementary material.

Conflicts of Interest: The authors declare no conflict of interest.

References

1. Hu, Z.; Zhu, Y.; Gao, Z.; Wang, G.; Liu, Y.; Liu, X.; Yuan, Z. CuO catalysts supported on activated red mud for efficient catalytic carbon monoxide oxidation. *Chem. Eng. J.* **2016**, *302*, 23–32. [[CrossRef](#)]
2. Pietrantonio, M.; Pucciarmati, S.; Torelli, G.N.; Aria, G.D.; Forte, F.; Fontana, D. Towards an integrated approach for red mud valorisation: A focus on titanium. *Int. J. Environ. Sci. Technol.* **2021**, *18*, 455–462. [[CrossRef](#)]
3. Evans, K. The history, challenges, and new developments in the management and use of bauxite residue. *J. Sustain. Metall.* **2016**, *2*, 316–331. [[CrossRef](#)]
4. Mayes, W.M.; Burke, I.T.; Gomes, H.I.; Anton, Á.D.; Molnár, M.; Feigl, V.; Ujaczki, É. Advances in understanding environmental risks of red mud after the ajka spill, hungary. *J. Sustain. Metall.* **2016**, *2*, 332–343. [[CrossRef](#)]
5. Luo, M.; Qi, X.; Zhang, Y.; Ren, Y.; Tong, J.; Chen, Z.; Hou, Y.; Yeerkebai, N.; Wang, H.; Feng, S.; et al. Study on dealkalization and settling performance of red mud. *Environ. Sci. Pollut. R.* **2017**, *24*, 1794–1802. [[CrossRef](#)]
6. Pepper, R.A.; Couperthwaite, S.J.; Millar, G.J. Value adding red mud waste: Impact of red mud composition upon fluoride removal performance of synthesised akaganeite sorbents. *J. Environ. Chem. Eng.* **2018**, *6*, 2063–2074. [[CrossRef](#)]
7. Li, H.; Xu, B.; Qi, F.; Sun, D.; Chen, Z. Degradation of bezafibrate in wastewater by catalytic ozonation with cobalt doped red mud: Efficiency, intermediates and toxicity. *Appl. Catal. B Environ.* **2014**, *152–153*, 342–351. [[CrossRef](#)]
8. Wang, L.; Sun, N.; Tang, H.; Sun, W. A review on comprehensive utilization of red mud and prospect analysis. *Minerals* **2019**, *9*, 362. [[CrossRef](#)]
9. Pande, G.; Selvakumar, S.; Ciotonea, C.; Giraudon, J.; Lamontier, J.; Batra, V.S. Modified red mud catalyst for volatile organic compounds oxidation. *Catalysts* **2021**, *11*, 838. [[CrossRef](#)]
10. Wu, J.; Gong, Z.; Lu, C.; Niu, S.; Ding, K.; Xu, L.; Zhang, K. Preparation and performance of modified red Mud-Based catalysts for selective catalytic reduction of NO_x with NH₃. *Catalysts* **2018**, *8*, 35. [[CrossRef](#)]
11. Joseph, C.G.; Taufiq-Yap, Y.H.; Krishnan, V.; Puma, G.L. Application of modified red mud in environmentally-benign applications: A review paper. *Environ. Eng. Res.* **2020**, *25*, 795–806. [[CrossRef](#)]
12. Ye, J.; Cong, X.; Zhang, P.; Hoffmann, E.; Zeng, G.; Liu, Y.; Fang, W.; Wu, Y.; Zhang, H. Interaction between phosphate and acid-activated neutralized red mud during adsorption process. *Appl. Surf. Sci.* **2015**, *356*, 128–134. [[CrossRef](#)]
13. Kim, S.C.; Nahm, S.W.; Park, Y. Property and performance of red mud-based catalysts for the complete oxidation of volatile organic compounds. *J. Hazard. Mater.* **2015**, *300*, 104–113. [[CrossRef](#)] [[PubMed](#)]
14. Ryu, S.; Lee, J.; Reddy Kannapu, H.P.; Jang, S.; Kim, Y.; Jang, H.; Ha, J.; Jung, S.; Park, Y. Acid-treated waste red mud as an efficient catalyst for catalytic fast pyrolysis of lignin and polypropylene and ozone-catalytic conversion of toluene. *Environ. Res.* **2020**, *191*, 110149. [[CrossRef](#)] [[PubMed](#)]
15. Xu, B.; Qi, F.; Sun, D.; Chen, Z.; Robert, D. Cerium doped red mud catalytic ozonation for bezafibrate degradation in wastewater: Efficiency, intermediates, and toxicity. *Chemosphere* **2016**, *146*, 22–31. [[CrossRef](#)]

16. Nayak, M.; Dhanarajan, G.; Dineshkumar, R.; Sen, R. Artificial intelligence driven process optimization for cleaner production of biomass with co-valorization of wastewater and flue gas in an algal biorefinery. *J. Clean. Prod.* **2018**, *201*, 1092–1100. [[CrossRef](#)]
17. Guo, C.; Tan, Y.; Yang, S.; Qian, Y. Development of phenols recovery process with novel solvent methyl propyl ketone for extracting dihydric phenols from coal gasification wastewater. *J. Clean. Prod.* **2018**, *198*, 1632–1640. [[CrossRef](#)]
18. Sun, W.; Sun, Y.; Zhu, H.; Zheng, H. Catalytic activity and evaluation of Fe-Mn@Bt for ozonizing coal chemical biochemical tail water. *Sep. Purif. Technol.* **2020**, *239*, 116524. [[CrossRef](#)]
19. Chen, J.; He, Z.; Ji, Y.; Li, G.; An, T.; Choi, W. OH radicals determined photocatalytic degradation mechanisms of gaseous styrene in TiO_2 system under 254 nm versus 185 nm irradiation: Combined experimental and theoretical studies. *Appl. Catal. B Environ.* **2019**, *257*, 117912. [[CrossRef](#)]
20. Jaafarzadeh, N.; Ghanbari, F.; Ahmadi, M. Efficient degradation of 2,4-dichlorophenoxyacetic acid by peroxymonosulfate/magnetic copper ferrite nanoparticles/ozone: A novel combination of advanced oxidation processes. *Chem. Eng. J.* **2017**, *320*, 436–447. [[CrossRef](#)]
21. Nobbs, J.; Tizaoui, C. A modified indigo method for the determination of ozone in nonaqueous solvents. *Ozone Sci. Eng.* **2014**, *36*, 110–120. [[CrossRef](#)]
22. Lin, Y.; Wang, W.; Pan, S.; Ho, C.; Chiang, P. Environmental impacts and benefits of organic Rankine cycle power generation technology and wood pellet fuel exemplified by electric arc furnace steel industry. *Appl. Energy* **2016**, *183*, 369–379. [[CrossRef](#)]
23. Qi, F.; Chu, W.; Xu, B. Catalytic degradation of caffeine in aqueous solutions by cobalt-MCM41 activation of peroxymonosulfate. *Appl. Catal. B Environ.* **2013**, *134–135*, 324–332. [[CrossRef](#)]
24. Gomes, J.; Costa, R.; Quinta-Ferreira, R.M.; Martins, R.C. Application of ozonation for pharmaceuticals and personal care products removal from water. *Sci. Total Environ.* **2017**, *586*, 265–283. [[CrossRef](#)]
25. Wang, J.; Bai, Z. Fe-based catalysts for heterogeneous catalytic ozonation of emerging contaminants in water and wastewater. *Chem. Eng. J.* **2017**, *312*, 79–98. [[CrossRef](#)]
26. Wang, Y.; Xie, Y.; Sun, H.; Xiao, J.; Cao, H.; Wang, S. 2D/2D nano-hybrids of $\gamma\text{-MnO}_2$ on reduced graphene oxide for catalytic ozonation and coupling peroxymonosulfate activation. *J. Hazard. Mater.* **2016**, *301*, 56–64. [[CrossRef](#)]
27. Tan, X.; Wan, Y.; Huang, Y.; He, C.; Zhang, Z.; He, Z.; Hu, L.; Zeng, J.; Shu, D. Three-dimensional MnO_2 porous hollow microspheres for enhanced activity as ozonation catalysts in degradation of bisphenol a. *J. Hazard. Mater.* **2017**, *321*, 162–172. [[CrossRef](#)] [[PubMed](#)]
28. Dai, Q.; Wang, J.; Yu, J.; Chen, J. Catalytic ozonation for the degradation of acetylsalicylic acid in aqueous solution by magnetic CeO_2 nanometer catalyst particles. *Appl. Catal. B Environ.* **2014**, *144*, 686–693. [[CrossRef](#)]
29. Huang, Y.; Cui, C.; Zhang, D.; Li, L.; Pan, D. Heterogeneous catalytic ozonation of dibutyl phthalate in aqueous solution in the presence of iron-loaded activated carbon. *Chemosphere* **2015**, *119*, 295–301. [[CrossRef](#)] [[PubMed](#)]
30. Van, H.T.; Nguyen, L.H.; Hoang, T.K.; Tran, T.P.; Vo, A.T.; Pham, T.T.; Nguyen, X.C. Using FeO-constituted iron slag wastes as heterogeneous catalyst for Fenton and ozonation processes to degrade Reactive Red 24 from aqueous solution. *Sep. Purif. Technol.* **2019**, *224*, 431–442. [[CrossRef](#)]
31. Bai, Z.; Yang, Q.; Wang, J. Catalytic ozonation of sulfamethazine using $\text{Ce}_{0.1}\text{Fe}_{0.9}\text{OOH}$ as catalyst: Mineralization and catalytic mechanisms. *Chem. Eng. J.* **2016**, *300*, 169–176. [[CrossRef](#)]
32. Audenaert, W.T.M.; Vandierendonck, D.; Van Hulle, S.W.H.; Nopens, I. Comparison of ozone and HO induced conversion of effluent organic matter (EfOM) using ozonation and UV/ H_2O_2 treatment. *Water Res.* **2013**, *47*, 2387–2398. [[CrossRef](#)]
33. Bai, Z.Y.; Yang, Q.; Wang, J.L. Fe_3O_4 /multi-walled carbon nanotubes as an efficient catalyst for catalytic ozonation of phydroxybenzoic acid. *Int. J. Environ. Sci. Technol.* **2016**, *13*, 483–492. [[CrossRef](#)]
34. Jothinathan, L.; Hu, J. Kinetic evaluation of graphene oxide based heterogenous catalytic ozonation for the removal of ibuprofen. *Water Res.* **2018**, *134*, 63–73. [[CrossRef](#)] [[PubMed](#)]
35. Wang, Y.; Yang, W.; Yin, X.; Liu, Y. The role of Mn-doping for catalytic ozonation of phenol using $\text{Mn}/\gamma\text{-Al}_2\text{O}_3$ nanocatalyst: Performance and mechanism. *J. Environ. Chem. Eng.* **2016**, *4*, 3415–3425. [[CrossRef](#)]
36. Yu, D.; Wu, M.; Hu, Q.; Wang, L.; Lv, C.; Zhang, L. Iron-based metal-organic frameworks as novel platforms for catalytic ozonation of organic pollutant: Efficiency and mechanism. *J. Hazard. Mater.* **2019**, *367*, 456–464. [[CrossRef](#)] [[PubMed](#)]
37. Zhang, T.; Li, W.; Croué, J. A non-acid-assisted and non-hydroxyl-radical-related catalytic ozonation with ceria supported copper oxide in efficient oxalate degradation in water. *Appl. Catal. B Environ.* **2012**, *121–122*, 88–94. [[CrossRef](#)]
38. Zhang, J.; Hu, Y.; Jiang, X.; Chen, S.; Meng, S.; Fu, X. Design of a direct Z-scheme photocatalyst: Preparation and characterization of $\text{Bi}_2\text{O}_3/g\text{-C}_3\text{N}_4$ with high visible light activity. *J. Hazard. Mater.* **2014**, *280*, 713–722. [[CrossRef](#)] [[PubMed](#)]
39. Sun, W.; Zhou, S.; Sun, Y.; Tang, J.; Zheng, H. Ozone catalytic oxidation capacity of Ti-Co@ Al_2O_3 for the treatment of biochemical tailwater from the coal chemical industry. *Water Environ. Res.* **2020**, *92*, 1283–1292.
40. Hu, E.; Wu, X.; Shang, S.; Tao, X.; Jiang, S.; Gan, L. Catalytic ozonation of simulated textile dyeing wastewater using mesoporous carbon aerogel supported copper oxide catalyst. *J. Clean. Prod.* **2016**, *112*, 4710–4718. [[CrossRef](#)]